

The influence of phosphorus precursor on the structure and properties of SiO₂-P₂O₅-CaO bioactive glass

Huihui Ren^{†,‡,1}, Yun Tian^{#,1}, Ailing Li[†], Richard A. Martin^{§,*} and Dong Qiu^{†,‡*}

[†]Beijing National Laboratory for Molecular Sciences, State Key Laboratory of Polymer Physics and Chemistry, Institute of Chemistry, Chinese Academy of Sciences, Beijing 100190, P.R. China

[‡] University of Chinese Academy of Sciences, Beijing 100190, P.R. China

[#] Orthopedic Department, Peking University Third Hospital, Beijing 100191, P.R. China

[§] Aston Institute of Materials Research and Aston Research Centre for Healthy Ageing, University of Aston, Birmingham, B4 7ET, UK.

*Corresponding authors.

E-mail address: r.a.martin@aston.ac.uk (R. A. Martin); dqiu@iccas.ac.cn (D. Qiu).

¹ These authors contributed equally to this work.

ABSTRACT

Bioactive glasses (BG) are one of the most promising bone regeneration materials because they can bond to bone and simulate new bone growth. Sol–gel methods for producing BG are well established, however challenges still remain in selecting and optimizing the precursors. Even for bioactive glasses with the same final composition, different precursors may lead to different structures and properties of the gel derived BG. In this work, three different phosphorus precursors, phytic acid (PA), triethyl phosphate (TEP) and n-butyl phosphate (BP) were used to prepare BG (54.2%SiO₂-35%CaO-10.8%P₂O₅, mol. %). The obtained materials were characterized by TGA, FTIR, XRD, HEXRD, solid state ³¹P, ²⁹Si NMR and by *in vitro* tests in SBF. It was found that the materials prepared by TEP or BP showed small amounts of crystallization, whereas the resulting material prepared by PA remained amorphous and had more P atoms as orthophosphate. *In vitro* assays indicated that all these materials were bioactive, while the BG prepared by PA showed the highest *in vitro* bioactivity, followed by TEP and, finally, BP. Based on these observations, it appears that phosphorus precursors have a significant impact on both the structure and bioactivity of the sol-gel derived BG. Results suggest that phytic acid should be used in preference to triethyl phosphate or n-butyl phosphate for the synthesis of sol gels. PA may improve the homogeneity of the sol gel glasses, reduce crystallization and lower stabilization temperatures.

KEYWORDS

Bioactive glasses; Phosphorus precursors; Structure; Bioactivity

1. Introduction

Developed around 40 years ago, bioactive glasses (BG) represent one of the most promising biomaterials for hard and soft tissue repair and engineering, owing to their excellent bioactivity, biocompatibility, osteoconductivity, and controllable physiochemical properties¹⁻⁴. When implanted, bioglass 45S5 bonds with bone rapidly and also stimulates bone growth away from the bone-implant interface^{5, 6}. Ions released from BG, especially soluble silicon, calcium and phosphorous ions, are known to stimulate osteoprogenitor cells at the genetic level and subsequently increase the rate of bone ingrowth^{1, 7}. BGs have therefore been widely used commercially for bone repair and dental applications^{8, 9}.

Sol-gel methods have been used to synthesize BGs since early 1990s¹⁰. Compared with traditional melt-quench methods that require very high processing temperatures (above 1300°C), the sol-gel technique allows BGs to be synthesized at much lower temperature based on a hydrolysis and condensation process^{10, 11}. Sol-gel derived BG tends to have nanometer-scale textural porosities, high specific surface area and numerous Si-OH groups on their surface, which makes them more bioactive and degrade more rapidly than the melt-derived analogues of a similar composition^{2, 11}. Additionally, the sol-gel process provides a versatile method to design or tailor BG with different structure, composition and morphology¹².

Different precursors have been used to prepare BG via the sol-gel methods². Studies have demonstrated that variations in the precursors could significantly affect

the process of synthesis, crystallization temperatures and the type of crystalline phases in the final products¹³⁻¹⁵. Nevertheless, challenges still remain in selecting and optimizing precursors in the sol–gel synthesis of BG. In the typical SiO₂-P₂O₅-CaO system, tetraethyl orthosilicate (TEOS) is commonly chosen as the precursor of silicon and triethyl phosphate (TEP) for phosphorus. Ca(NO₃)₂·4H₂O usually serves as the precursor of calcium since it is highly soluble in the reaction medium and easy to handle. However, some issues still remain in this system due to the poor compatibility between calcium and the phosphorus precursors (TEP). It has been shown that the phosphorus precursors with formula PO(OR)₃ (i.e. TEP) have high stability against hydrolysis¹⁶. More importantly, calcium does not enter the silicate network until heat-treated above 350°C in this system¹⁷⁻¹⁹. Toxic nitrate ions are not completely removed until heat treating at temperatures of 500°C or above^{17, 18, 20}. Although calcium 2-methoxyethoxide (CME), another potential calcium precursor, has been explored to incorporate calcium into the silicate network at low temperature (below 60 °C), its use is still limited due to its extremely high sensitivity to water²¹⁻²³.

It has also been suggested that PO(OR)_x(OH)_{3-x} (x=1, 2) is a better phosphorus precursor for sol–gel synthesis^{16, 24}. In our previous studies, phytic acid (PA), C₆H₁₈O₂₄P₆, a member of the PO(OR)_x(OH)_{3-x} family, was used as phosphorus precursor to prepare SiO₂-P₂O₅-CaO BG²⁵. It was found that PA not only helps the incorporation of calcium into the phosphosilicate network at a relatively low temperature, but also enables the production of calcium phosphosilicate gels over a broad compositional range. Therefore, it is possible that for sol-gel derived glasses with

the same final composition, different phosphorus precursor may result in different structures in the final BG and thus affect its biological properties.

The aim of the present work is to study the influence of phosphorus precursors on the structure and bioactivity of a newly developed BG (54.2%SiO₂-35%CaO-10.8%P₂O₅, mol. %). TEP, PA, and another member of the PO(OR)_x(OH)_{3-x} family, n-butyl phosphate (BP) were chosen as phosphorus precursors. Thermogravimetric analysis (TGA), Fourier transform infrared spectroscopy (FTIR), X-ray diffraction (XRD), high-energy X-ray diffraction (HEXRD) and solid state NMR were used to characterize the structures of these samples. Their *in vitro* bioactivities were evaluated by immersing in simulated body fluid (SBF).

2. 2. Materials and Methods

2.1 Materials

Phytic acid (50 wt% aqueous solution) was purchased from Sigma-Aldrich (St. Louis, MO, USA). Tetraethyl orthosilicate (TEOS, ≥ 99.0%), triethyl phosphate (TEP, ≥ 99.5%) and Ca(NO₃)₂·4H₂O were purchased from Sinopharm Chemical Reagent (Beijing, China). n-Butyl phosphate (BP, mixture of mono-n-butyl and di-n-butyl with 1:1 molar ratio) was purchased from Alfa Aesar. All reagents were used as received.

2.2 Preparation of BG

BG with the composition of 54.2%SiO₂-35%CaO-10.8%P₂O₅ (mol. %) were synthesized by sol-gel methods using PA, TEP, BP as the phosphorus precursors,

respectively. This BG composition was chosen because it showed excellent bioactivity and could maintain a stable pH when reacting with physiological solution.

These samples were prepared as previously described^{18, 25}. When PA was used as the phosphorus precursor, it was mixed with ethanol and deionized water at room temperature, then TEOS was added under magnetic stirring. After 1h, $\text{Ca}(\text{NO}_3)_2 \cdot 4\text{H}_2\text{O}$ powders were added into the mixed solution and stirred vigorously until a transparent solution was formed (the sol). For TEP, under constant stirring, the pre-calculated TEOS, TEP and $\text{Ca}(\text{NO}_3)_2 \cdot 4\text{H}_2\text{O}$ were sequentially added into a solution of HNO_3 , ethanol and water. HNO_3 was used as catalyst with a molar ratio of $\text{HNO}_3/(\text{TEOS}+\text{TEP}) = 1/20$. The same procedure for TEP was also employed for BP. All of the sols were left to gel at ambient temperature, then aged at 60°C for 1 week, dried at 120°C for another 1 week and finally sintered at 400°C for 2h. The obtained BG powders were ground to form particles of size $< 38\mu\text{m}$ for further study. The samples prepared from PA, TEP, BP are referred to as PA-BG, TEP-BG, BP-BG, respectively.

2.3 Characterization of the materials

Thermogravimetric analysis (TGA)

Thermogravimetric measurements were undertaken on these gels, after drying at 120°C , using a Pyris 1 TGA instrument. The samples ($\sim 5\text{mg}$) were measured with a $5^\circ\text{C}/\text{min}$ heating rate under an air atmosphere and data was collected from 50°C to 700°C . The differential curves of the TGA data were obtained by using Origin software.

Fourier transform infrared spectroscopy (FTIR)

The FTIR analysis of all the samples were measured on a Bruker Equinox 55 instrument. All samples were diluted with KBr, finely powdered and pressed into pellets. The spectra were collected in the range 2000-400 cm^{-1} at a 4 cm^{-1} resolution with an average value of 32 scans and analyzed utilizing the OPUS software version 4.0.

X-ray diffraction (XRD)

XRD measurements were carried out using a Rigaku (D/MAX 2500) instrument with Cu K α radiation ($\lambda = 1.54 \text{ \AA}$) operated at 40 kV and 200 mA. The powder XRD data was collected at diffraction angles (2θ) from 10° to 70° with a scanning speed of $4^\circ/\text{min}$.

High-energy X-ray diffraction (HEXRD)

The HEXRD data were collected on station BL13W1 at Shanghai Synchrotron Radiation Facility (SSRF), P.R. China. The finely ground samples were packed into a cylindrical container of 0.5mm internal diameter and the energy was set as 17.43 keV (X-ray wavelength: 0.7113 \AA). The data were collected at scattering angles (2θ) from 2° to 108.35° with a scanning step of 0.05° and a counting time of 2s per point. The data corrections were performed on a program written in-house, involving the removal of background scattering, polarization correction, absorption correction, volume correction and normalization process. Following these corrections, the resultant interference function, $i(Q)$, could be obtained. Fourier transformation of $i(Q)$ generates the pair distribution functions (PDFs, $T(r)$), which can be used to describe the structure

of amorphous materials.

$$T(r) = T^0(r) + \int_0^\infty Qi(Q)M(Q) \sin(Qr)dQ$$

where $T^0(r) = 2\pi^2 r \rho_0$ (r is the atomic separation between atoms and ρ_0 is the number density); $M(Q)$ is a window function that mitigates the effect of the finite maximum experimentally attainable value of Q . The associated structural parameters i.e., atomic distances and coordination numbers, were given by simulating PDFs using the NXFit program²⁶.

Solid state NMR

Solid state ^{31}P NMR and ^{29}Si NMR spectroscopy were measured using a Bruker Avance III 400 MHz instrument providing the following Larmor frequencies: 161.58 MHz for ^{31}P and 79.30 MHz for ^{29}Si . The experiments were conducted at a spinning speed of 12 kHz for ^{31}P and 8 kHz for ^{29}Si , respectively. The ^{31}P and ^{29}Si NMR spectra were referenced using ammonium dihydrogen phosphate ($\text{NH}_4\text{H}_2\text{PO}_4$) and tetramethylsilane (TMS), respectively.

2.4 Bioactivity test *in vitro*

Bioactivity of the obtained BG powders were tested *in vitro* by immersing in SBF at $36.5 \pm 0.5^\circ\text{C}$ ²⁷. In brief, SBF was prepared by dissolving reagents NaCl, NaHCO_3 , KCl, $\text{K}_2\text{HPO}_4 \cdot 3\text{H}_2\text{O}$, $\text{MgCl}_2 \cdot 6\text{H}_2\text{O}$, CaCl_2 , and Na_2SO_4 in deionized water. The solution was buffered to pH 7.4 with Tris- (hydroxymethyl)-aminomethane ($(\text{CH}_2\text{OH})_3\text{CNH}_2$) and

hydrochloric acid to give a resultant ion concentration similar to human plasma. 150 mg of each powder ($<38\ \mu\text{m}$) was immersed in 100 mL of SBF. After immersing for selected time intervals, the powders in SBF were isolated by centrifugation, rinsed gently with pure water and dried in a desiccator. Formation of hydroxyapatite (HA) was monitored by SEM, XRD and FTIR. The pH change of the solution after the powders were immersed for specified time intervals was also examined by a pH monitor (PB-10).

3. Results and Discussion

3.1 The chemical and structural characterization

TGA curves of the sol gels prepared by different phosphorus precursors are shown in Figure 1. For TEP-BG and BP-BG, the gels underwent two obvious weigh loss stages at ~ 200 to 300°C and 500 to 600°C before becoming stable. The first stage may be associated with the loss of organic moieties and the removal of some nitrate ions by means of their thermal degradation. The latter stage was primarily ascribed to the decomposition of residual calcium nitrate and partly to the dehydroxylation, which is

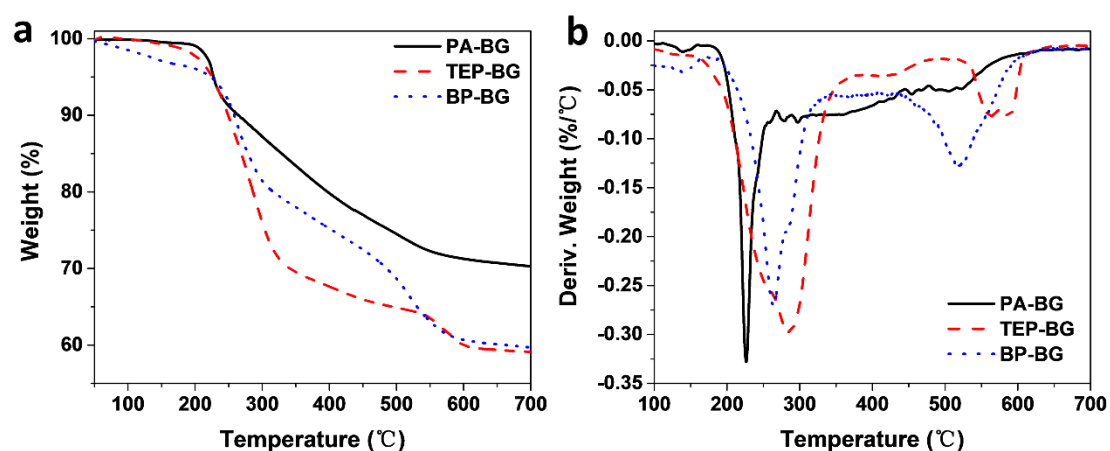


Figure 1. (a) TGA curves of the BG gels after drying at 120°C and (b) their corresponding differential curves.

consistent with previous observations for similar materials^{17, 18, 28}. While for PA-BG, there was a rapid weight loss at approximately 240°C, after which the change of weight became slower and slower until reaching relatively steady state. The weight loss stage between 500 ~ 600°C was not apparent, which means all or most of nitrates have been decomposed before this stage. This phenomena is presumably owing to the good affinity of PA to calcium ions, facilitating the breaking down of calcium nitrate. Additionally, according to previous studies, calcium did not enter the silicate network (i.e. S70C30 system) until heat-treated beyond 350°C^{17, 18, 29}. Based on these results, the gels were heat treated at 400°C for further study.

Figure 2 shows the FTIR and XRD spectra of the BG powders after heat treatment at 400°C for 2h. It can be seen that all the FTIR spectra showed the typical bands for sol-gel glasses. The bands at 1000-1100 cm⁻¹ correspond to the asymmetric stretching vibrations of SiO₄ and PO₄ tetrahedrons. The peak at 800 cm⁻¹ is assigned to symmetric stretching vibration Si–O–Si (s, sym) and the peak at 467 cm⁻¹ is associated to rocking vibration Si–O–Si (r)³⁰. The shoulder at 940 cm⁻¹ is related to the non-bridging bonds

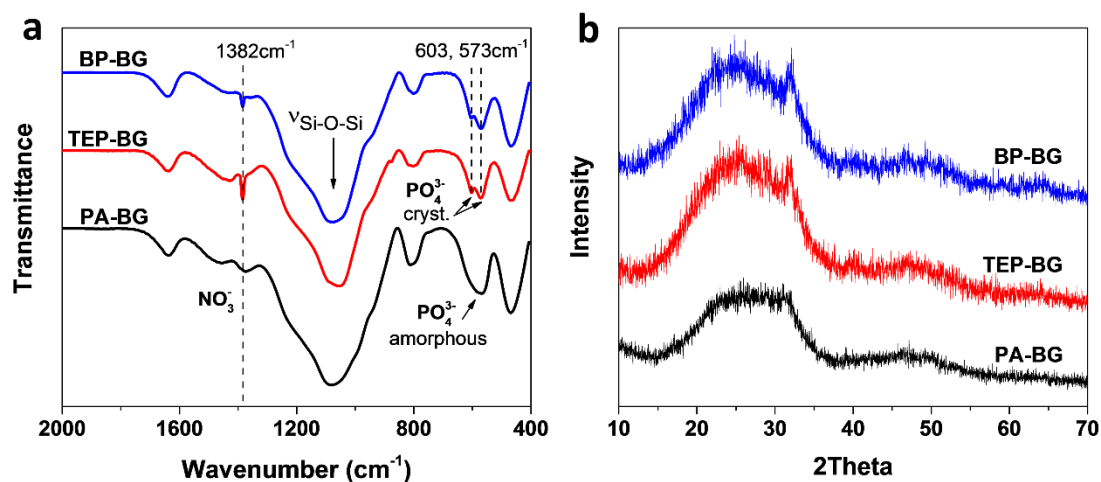


Figure 2. (a) FTIR and (b) XRD spectra of the BG powders after heat treatment at 400°C.

of Si–O–X (X=Ca, H)^{17, 30}.

Nevertheless, there were some important difference between the FTIR spectra of the samples. In the case of TEP-BG and BP-BG, two peaks at 573 cm⁻¹ and 603 cm⁻¹ appeared on the FTIR spectra. The double peaks assigned to the bending vibration P–O are a characteristic feature of crystalline phosphates³¹. However, for PA-BG, there is only one peak in this region, which is commonly corresponded to phosphate in amorphous phase¹⁴. Correspondingly, XRD patterns of TEP-BG and BP-BG have a small peak at around 32°, indicating partial crystallization. No peak are present in the XRD spectrum of PA-BG, indicating that it remained amorphous.

It was also worthy to note the sharp peak at 1382 cm⁻¹ on the FTIR spectra that was assigned to nitrate ions³¹. This peak appeared on the FTIR spectra of TEP-BG and BP-BG but not on PA-BG. This suggests that after heat treatment at 400°C the nitrate ions had been entirely removed from PA-BG whilst some of them still remained in the TEP-BG and BP-BG samples. These results are in agreement with the TGA data and previous studies, in which the entire removal of nitrate ions requires heat treatment at 500°C or above in the system with no phosphorus precursor or using TEP as phosphorus precursor^{17, 18, 20}. These observations suggest that using PA as the phosphorus precursor is favorable to the decomposition of calcium nitrate at a relatively low temperature when compared to using TEP or BP.

In addition, when thermally treated at 600°C, PA-BG still remained amorphous and TEP-BG and BP-BG showed partial crystallization (figure S1, supporting

information). Correspondingly, after calcining at 600°C, the sharp peak assigned to nitrate ions (1382 cm⁻¹) disappeared for all of the glasses, suggesting the remove of all the nitrate ions.

For amorphous materials, HEXRD experiments are frequently used to provide structural information at the atomic scale. The real-space pair distribution functions (PDFs, $T(r)$) can be obtained by Fourier transformation of HEXRD data and by simulating PDFs, the associated structural parameters i.e., atomic distances and coordination numbers, could be obtained. As shown in figure 3 and table 1, PDFs of all samples showed similar structural features of BG: a correlation peak at ~1.6 Å is assigned to P-O and Si-O bonds and a peak at ~2.5 Å mainly corresponded to Ca-O and O-O (O-Si-O and O-P-O) bonds^{20, 32}. However, no obvious difference were found among these three samples. This is mainly because the information given by PDFs was

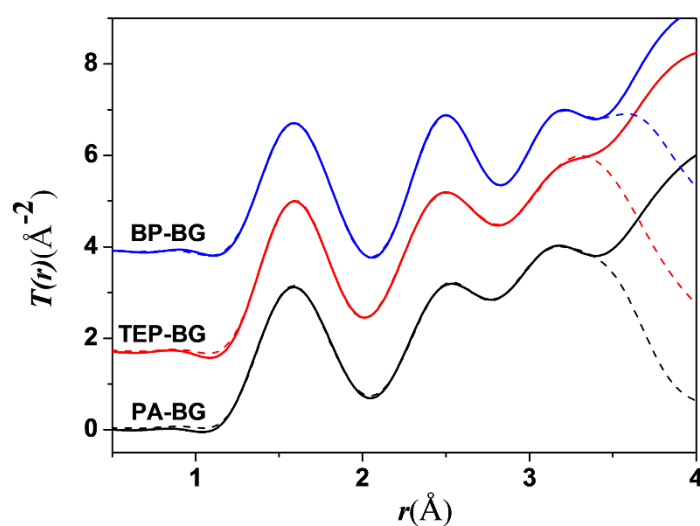


Figure 3. The real-space pair distribution functions (solid lines), $T(r)$, obtained by Fourier transformation of HEXRD data together with their simulations (dashed lines).

Table 1. Structural parameters obtained from the simulation of HEXRD data*.

Correlation	PA-BG		TEP-BG		BP-BG	
	r(Å) (± 0.02)	N (± 0.2)	r(Å) (± 0.02)	N (± 0.2)	r(Å) (± 0.02)	N (± 0.2)
P-O	1.52	4.1	1.54	4.2	1.54	4.1
Si-O	1.61	4.1	1.60	4.2	1.61	4.2
Ca-O	2.45	5.4	2.42	5.6	2.43	5.5
O-O	2.60	4.7	2.59	4.8	2.60	4.7

* r is the atomic separation, N is the coordination number. The errors are reasonably estimated as $\pm 0.02\text{\AA}$ in r and ± 0.2 in N.

statistically averaged. In these mixed phosphate-silicate networks, even with network modifiers, the significant overlap between different pairwise correlations made it impossible for PDFs to unambiguously characterize the structure. Although a slightly shorter P-O bond length was observed for PA-BG (Table 1), the difference was very small considering the uncertainty of these parameters ($\pm 0.02\text{\AA}$). Additionally, considering the lower content of phosphorous in these materials, the error associated with P-O bond length could be even greater. In brief, for these samples prepared by different phosphorus precursors, the HEXRD data gave the overall characteristics of the structure, but cannot clearly distinguish the difference among their structures. To give a better understanding of their structures, other spectroscopic techniques were therefore also required.

A combination of solid state ^{31}P NMR and ^{29}Si NMR techniques were used to explore structure of these samples. The ^{31}P , ^{29}Si NMR spectra and the deconvoluted peaks are shown in Figure 4. The respective peak chemical shifts and relative populations of the Q^n units are summarized in Table 2. The Q^n unit represents a Si-O tetrahedron (or P-O

tetrahedron) bonded to n bridging oxygen (BO) and (4-n) non-bridging oxygen (NBO) atoms. For PA-BG, ^{31}P NMR spectrum showed a main peak at $\sim 2\text{ppm}$ and a minor peak at $\sim -7.5\text{ppm}$, which were assigned to Q_p^0 and Q_p^1 units, respectively³³. This suggests that the majority of phosphorus atoms were present as orthophosphate (Q_p^0 units, PO_4 , 74%) with the remainder present as P-O-X (X = P or Si, Q_p^1 units). In this case, although ^{31}P NMR spectra confirmed the existence of ^{31}P in Q_p^1 units, it cannot discriminate whether ^{31}P was present as P-O-P or P-O-Si. Similar Q_p^1 NMR signals had sometimes been suggested to attribute to pyrophosphates (i.e., P-O-P bonds)³⁴. On the other hand, it has been suggested that in $\text{CaO-SiO}_2\text{-P}_2\text{O}_5$ glasses this signal might represent P-O-Si moieties³⁵. For TEP-BG and BP-BG, three resonances at approximately 2, -8 and -24ppm were present on the ^{31}P NMR spectra. These resonances can be assigned to ^{31}P in Q^0 , Q^1 and Q^2 structural units, respectively³³. Compared to PA-BG, the TEP-BG and BP-BG samples had a lower fraction of Q_p^0 units, a higher fraction of Q_p^1 and Q_p^2 units (table 2). Considering the charge-balancing, these results indicated that there were more Ca^{2+} connected to phosphorus in PA-BG. This should be mainly due to the different affinity of these phosphorus precursors with calcium.

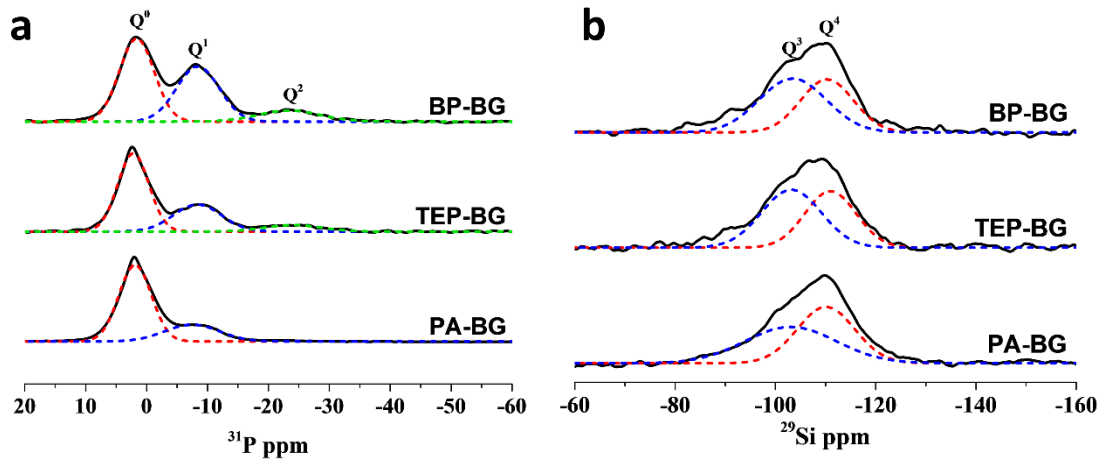


Figure 4. Solid state ^{31}P NMR and ^{29}Si NMR spectroscopy (solid curves) of the samples after heat treatment at 400°C . The component peaks obtained by fitting the experimental spectra are shown in dash lines.

Table 2. ^{31}P and ^{29}Si Chemical Shifts and Relative Populations of Q^n Units.

Samples	Q_P^0		Q_P^1		Q_P^2		Q_{Si}^3		Q_{Si}^4	
	δ/ppm	P/%								
PA-BG	1.9	74	-7.5	26	--	--	-103.0	51	-110.0	49
TEP-BG	2.2	59	-8.3	32	-24.1	9	-103.2	55	-111.0	45
BP-BG	1.6	49	-8.4	40	-23.4	12	-103.5	56	-110.3	44

From figure 4b, it can be seen that all samples have similar ^{29}Si NMR spectra, mainly consisted of Si in Q^4 and Q^3 units. Whilst melt-quenching glasses typically consist of Q_{Si}^2 and Q_{Si}^3 units^{3,34}, Q^4 and Q^3 units are usually present in sol-gel silicate materials^{29, 36}. As mentioned above, calcium enter the phosphosilicate network after heat treatment. Generally, charge balance arguments would lead to less Si-O-Ca bond formation (i.e. Q_{Si}^3 units) as more Ca^{2+} will be connected to phosphorus. Gaussian fitting results showed that there were a slightly less Q_{Si}^3 units in PA-BG (table 2), in agreement with the ^{31}P NMR results. Furthermore, numerous Si-O-H bonds are still present in these sol-gel glasses even after heat treatment. Thus, H^+ is also likely to act

as a network modifier to balance the negative charges by forming NBOs in these systems.

It is well known that different polymorphs exist for crystalline materials of a fixed stoichiometry and that this can influence dissolution and bioactivity, e.g. tri-calcium phosphate (TCP) alpha and beta phases where TCP- α is more soluble and reactive than TCP- β . However, due to their lack of long range order and isotropic nature glasses are widely assumed to adopt structures that are solely determined by their composition. Whilst this may be true to melt-quench derived glasses the present study shows that important structural differences may be present in sol-gel derived glasses with the same composition.

3.2 *In vitro* assay in SBF

As discussed above, phosphorus precursors significantly affect the structure of SiO₂-P₂O₅-CaO gel-glasses, especially the phosphorus environment. It is known that the composition and structure are critical for their bioactivity³. Thus, the samples prepared by different phosphorus precursors may exhibit different bioactivity. The bioactivity of these samples were tested by immersing them in SBF and the results are shown in figures 5 and 6. For sample PA-BG, a layer consisting of needle like aggregates covered almost the entire surface after 12h immersion (figure 5b). At 24h, the layer entirely covered the surface and showed a typical morphology of HA^{14, 22} (figure 5c). The formation of HA were also confirmed by XRD and FTIR (figure 6a and figure 6d). The XRD spectra (figure 6a) showed characteristic HA diffraction peaks (25.9, 31.7, 32.8,

39.7, 46.6, 49.4, 53.2 and 64.1°, PDF#09-0432) which appeared and became stronger with immersion time. Correspondingly, with increasing immersion time, the appearance of peaks at 607 and 567 cm^{-1} (δ P–O, crystal) and an increase in 960 cm^{-1} band intensity (ν_s P–O) on the FTIR spectra were also observed due to the formation of HA (figure 6d).

For TEG-BG and BP-BG samples the confirmation of the precipitated HA by FTIR was not as obvious, primarily because there is already some crystalline phosphate in the original BGs. However needle-like precipitates are observed on their surface (figure 5d-i) and the characteristic diffraction peaks corresponded to HA (PDF#09-0432) on the XRD spectra (figure 5b-c) confirm the formation of HA. Nevertheless, compared to PA-BG, whose surface was entirely covered by HA after 24h (figure 5c), the surfaces of these two samples were only partially covered by HA after 24h (figure 5f, 5i). Meanwhile, the intensity of HA peaks related to PA-BG after 24h immersion were also stronger than those of the other two samples (TEP & BP), indicating that PA-BG has a better bioactivity.

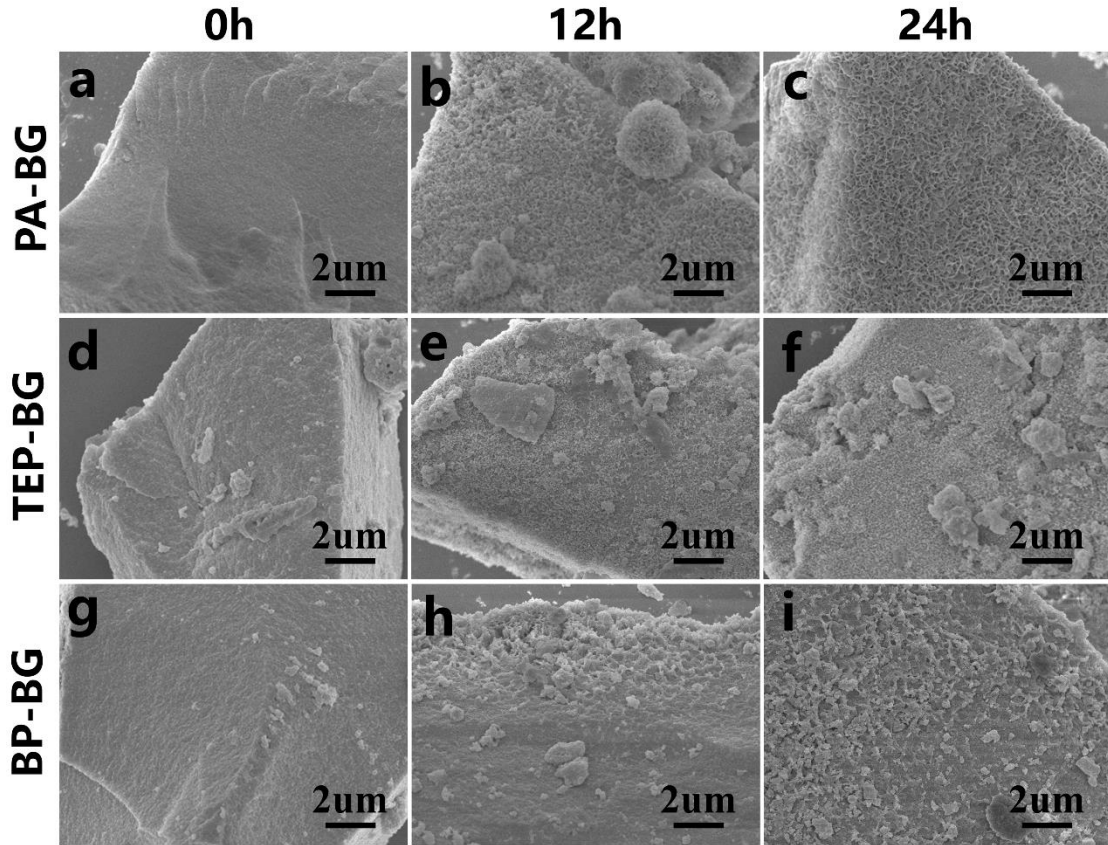


Figure 5. SEM images of surface morphologies of the samples before and after immersion in SBF for different times. (a, b, c): PA-BG; (d, e, f): TEP-BG; (g, h, i): TEP-BG;

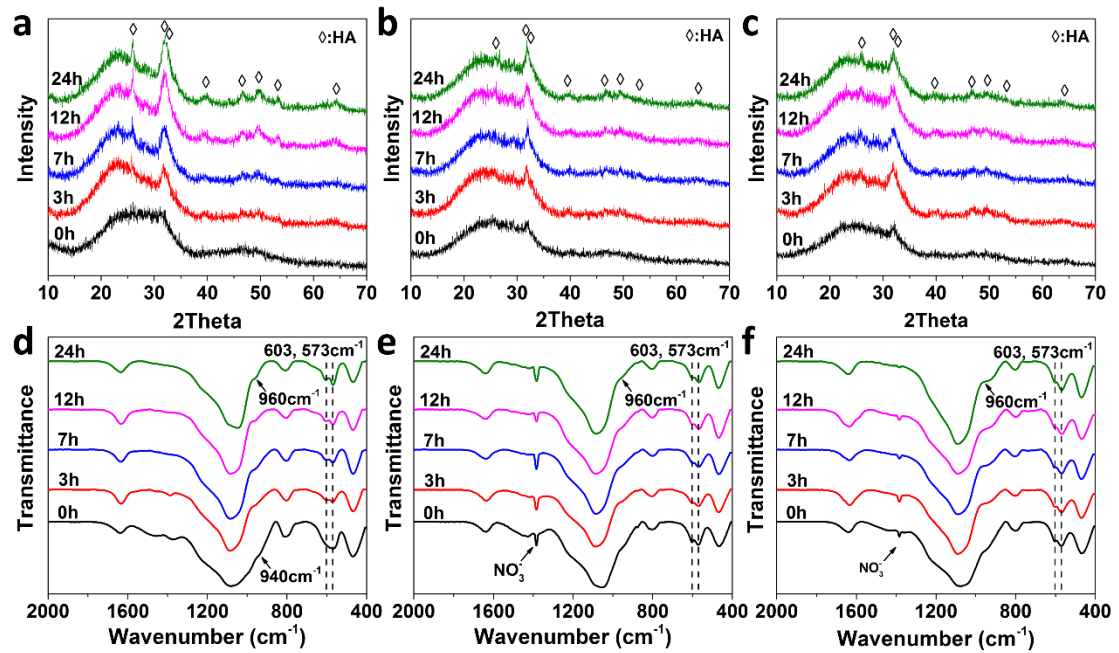


Figure 6. XRD patterns and FTIR spectra of the samples after immersion in SBF for 0h, 3h, 7h, 12h and 24h. (a, d): PA-BG; (b, e): TEP-BG; (c, f): TEP-BG;

Figure 7 gives an approximate comparison of the *in vitro* bioactivity of the samples. In figure 7, S_a represents the area of amorphous scattering peak and S_b represents the area of the crystallization peaks in the corresponding region. To a first approximation the ratio of S_b/S_a reflects the relative amount of the precipitated HA. According to figure 7, the S_b/S_a follows such as order: PA-BG ($\sim 30\%$) > TEP-BG ($\sim 19\%$) > BP-BG ($\sim 12\%$), suggesting that PA-BG had the highest *in vitro* bioactivity whereas BP-BG had the lowest. Furthermore, the additional HA peaks at $\sim 39, 47, 49, 53$ and 64° are significantly larger for the PA-BG compared to the others.

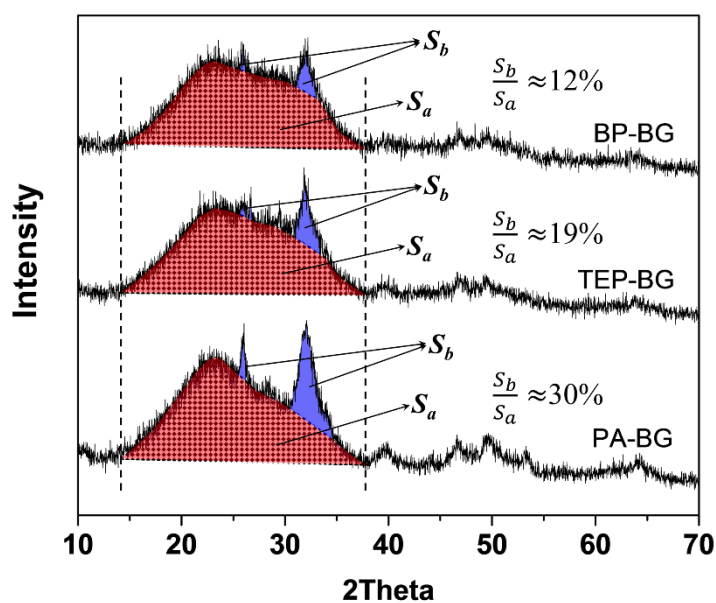


Figure 7. An approximate comparison of the *in vitro* bioactivity of the samples. XRD spectra: XRD spectra of the samples after immersion in SBF for 24h; S_a : the area of amorphous scattering peak; S_b : the area of the crystallization peaks in the corresponding region.

A stable pH in reacting with body fluid or SBF is one of the characteristics of this BG. The pH values of the SBF during the sample immersion are shown in figure 8. These three samples all showed a relatively constant pH compared to 45S5. This is due to the lack of sodium in the present composition and the relatively high content of phosphorus which produces acidic species helping to compensate for the pH increase caused by Ca^{2+} ^{33, 37}. It was also found that the pH of the solution for PA-BG was slightly lower than that of the other two samples, however, the difference is not significant. This suggests that the pH of BG in SBF is mainly determined by chemical composition.

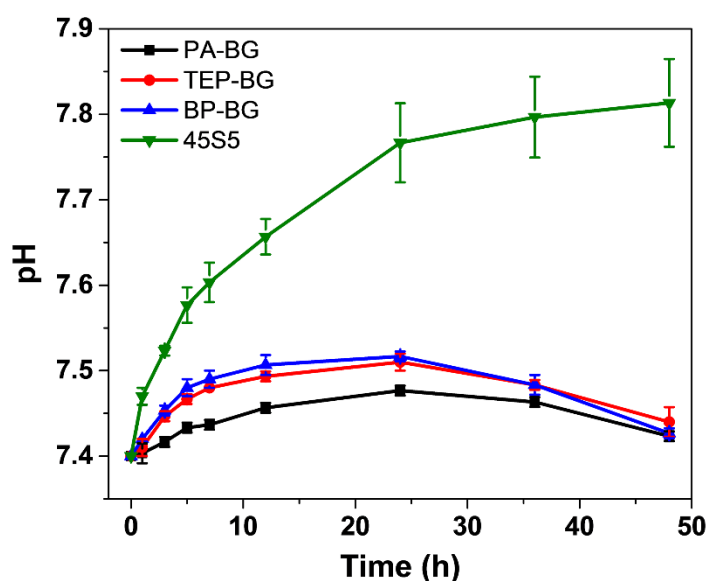


Figure 8. pH change of the SBF during the samples immersion within 48h.

4. Conclusions

In this study, $\text{SiO}_2\text{-P}_2\text{O}_5\text{-CaO}$ bioactive glasses were synthesized using PA, TEP and BP as the phosphorus precursor, respectively. The influence of phosphorus precursors on the structure and bioactivity of the resulting materials was evaluated. The chemical

and structural characterization showed that phosphorus precursors significantly affect the structure of the resulting materials, especially for the phosphorus environment. After heat treatment, a small amount of crystalline-phase were present in TEP-BG and BP-BG, whereas the PA-BG remained amorphous and more P atoms were present as orthophosphate (Q^0 units). The results of *in vitro* tests indicated that the bioactivity of these materials was also related with the phosphorus precursors. Although these materials all exhibited strong *in vitro* bioactivity, PA-BG showed the highest *in vitro* bioactivity, followed by TEP-BG and, finally, BP-BG. Phytic acid is a suitable phosphorous precursor for synthesizing bioactive sol-gels and potentially low temperature hybrids (e.g. poly-ethylene glycol, organic – inorganic hybrids).

Acknowledgements

This work was supported by National Natural Science Foundation of China (Grant No.: 81470101 and 51473004), the Strategic Priority Research Program of the Chinese Academy of Sciences (Grant No. XDB12020300) and a Royal Society/Natural Science Foundation of China international exchange grant (IE131323, 513111170).

Conflicts of Interest

None of the authors have any conflicts of interest.

References

1. L. L. Hench, *J. Mater. Sci.: Mater. Med.*, 2006, **17**, 967-978.
2. J. R. Jones, *Acta Biomater.*, 2013, **9**, 4457-4486.
3. D. S. Brauer, *Angew. Chem. Int. Ed.*, 2015, **54**, 4160-4181.
4. L. L. Hench, Splinter, R. J., Allen, W. C. and Greenlee, T. K., *Journal of Biomedical Materials Research Symposium*, 1971, **5**, 25.
5. J. R. Jones, *Acta Biomaterialia*, 2013, **9**, 4457-4486.
6. L. L. Hench, *Journal of Materials Science-Materials in Medicine*, 2006, **17**, 967-978.
7. I. D. Xynos, A. J. Edgar, L. D. K. Buttery, L. L. Hench and J. M. Polak, *Biochem. Biophys. Res. Commun.*, 2000, **276**, 461-465.
8. J. R. Jones, D. S. Brauer, L. Hupa and D. C. Greenspan, *Int. J. Appl. Glass Sci.*, 2016, **7**, 423-434.
9. A. Polini, H. Bai and A. P. Tomsia, *Wiley Interdiscip. Rev.: Nanomed. Nanobiotechnol.*, 2013, **5**, 399-410.
10. R. Li, A. E. Clark and L. L. Hench, *J. Appl. Biomater.*, 1991, **2**, 231-239.
11. D. Arcos and M. Vallet-Regí, *Acta Biomater.*, 2010, **6**, 2874-2888.
12. M. Vallet-Regí, A. J. Salinas and D. Arcos, *Int. J. Appl. Glass Sci.*, 2016, **7**, 195-205.
13. M. Łączka, K. Cholewa-Kowalska, K. Kulgawczyk, M. Klisch and W. Mozgawa, *J. Mol. Struct.*, 1999, **511**, 223-231.
14. R. L. Siqueira and E. D. Zanotto, *J. Mater. Sci.: Mater. Med.*, 2013, **24**, 365-379.
15. N. Shankhwar, G. P. Kothiyal and A. Srinivasan, *RSC Adv.*, 2015, **5**, 100762-100768.
16. D. Carta, D. M. Pickup, J. C. Knowles, M. E. Smith and R. J. Newport, *J. Mater. Chem.*, 2005, **15**, 2134-2140.
17. S. Vecchio Cipriotti and M. Catauro, *J. Therm. Anal. Calorim.*, 2015, **123**, 2091-2101.
18. M. Catauro, A. Dell'Era and S. Vecchio Cipriotti, *Thermochim. Acta*, 2016, **625**, 20-27.
19. V. FitzGerald, R. A. Martin, J. R. Jones, D. Qiu, K. M. Wetherall, R. M. Moss and R. J. Newport, *J. Biomed. Mater. Res., Part A*, 2009, **91A**, 76-83.
20. R. A. Martin, S. Yue, J. V. Hanna, P. D. Lee, R. J. Newport, M. E. Smith and J. R. Jones, *Phil. Trans. R. Soc. A*, 2012, **370**, 1422-1443.
21. B. Yu, C. A. Turdean-Ionescu, R. A. Martin, R. J. Newport, J. V. Hanna, M. E. Smith and J. R. Jones, *Langmuir*, 2012, **28**, 17465-17476.
22. A. Li, H. Shen, H. Ren, C. Wang, D. Wu, R. A. Martin and D. Qiu, *J. Mater. Chem. B*, 2015, **3**, 1379-1390.
23. Y. S. Sun, A. L. Li, F. J. Xu and D. Qiu, *Chin. Chem. Lett.*, 2013, **24**, 170-172.
24. D. M. Pickup, P. Guerry, R. M. Moss, J. C. Knowles, M. E. Smith and R. J. Newport, *J. Mater. Chem.*, 2007, **17**, 4777-4784.
25. A. L. Li and D. Qiu, *J. Mater. Sci.: Mater. Med.*, 2011, **22**, 2685-2691.
26. D. Pickup, R. Moss and R. Newport, *J. Appl. Crystallogr.*, 2014, **47**, 1790-1796.
27. T. Kokubo and H. Takadama, *Biomaterials*, 2006, **27**, 2907-2915.
28. Y.-S. Sun, A.-L. Li, H.-H. Ren, X.-P. Zhang, C. Wang and D. Qiu, *Chin. Chem. Lett.*, 2016, **27**, 579-582.
29. S. Lin, C. Ionescu, K. J. Pike, M. E. Smith and J. R. Jones, *J. Mater. Chem.*, 2009, **19**, 1276.
30. J. Ma, C. Z. Chen, D. G. Wang, X. G. Meng and J. Z. Shi, *Ceram. Int.*, 2010, **36**, 1911-1916.
31. M. Catauro, F. Bollino, R. A. Renella and F. Papale, *Ceram. Int.*, 2015, **41**, 12578-12588.

32. R. A. Martin, H. L. Twyman, G. J. Rees, J. M. Smith, E. R. Barney, M. E. Smith, J. V. Hanna and R. J. Newport, *Phys. Chem. Chem. Phys.*, 2012, **14**, 12105-12113.
33. F. Döhler, A. Mandlule, L. van Wüllen, M. Friedrich and D. S. Brauer, *J. Mater. Chem. B*, 2015, **3**, 1125-1134.
34. I. Elgayar, A. E. Aliev, A. R. Boccaccini and R. G. Hill, *J. Non-Cryst. Solids*, 2005, **351**, 173-183.
35. E. Leonova, I. Izquierdo-Barba, D. Arcos, A. Lopez-Noriega, N. Hedin, M. Vallet-Regi and M. Eden, *J. Phys. Chem. C*, 2008, **112**, 5552-5562.
36. Z. Lin, J. R. Jones, J. V. Hanna and M. E. Smith, *Phys. Chem. Chem. Phys.*, 2015, **17**, 2540-2549.
37. S. Padilla, J. Roman, A. Carenas and M. Vallet-Regi, *Biomaterials*, 2005, **26**, 475-483.